Advances in Differential Equations and Control Processes 2026, 33(3), 4535.
doi: https://doi.org/10.59400/adecp4535

Article

Online non-intrusive grid impedance estimation method for energy storage converters

Yunkun Xiang, **Kai Liu***, **Cheng Wan**, **Hao Zhou**, **Zipeng Hu**

State Grid Hunan Integrated Energy Service Co., Ltd., Changsha 410007, China; xiangyk2@hn.sgcc.com.cn (YX); wanc3@hn.sgcc.com.cn (CW); zhouh39@hn.sgcc.com.cn (HZ); huzp6@hn.sgcc.com.cn (ZH)

*** Corresponding authors:** Kai Liu, liuk43@hn.sgcc.com.cn

CITATION

Xiang Y, Liu K, Wan C, et al. Online non-intrusive grid impedance estimation method for energy storage converters. Advances in Differential Equations and Control Processes. 2026; 33(3): 4535. https://doi.org/10.59400/adecp4535

ARTICLE INFO

Received: 19 June 2026
Revised: 18 August 2026
Accepted: 23 February 2026
Available online: 27 February 2026

Abstract: Grid impedance has an important influence on the synchronization stability of grid-connected energy storage converters and their adaptability to weak grids. Conventional intrusive estimation methods require additional perturbations to be injected, which reduces power quality and complicates practical applications. This paper proposes a non-intrusive online grid impedance estimation method. The excitation source is the power regulation dynamics of the energy storage converter itself. The sliding-window discrete Fourier transform is used to extract the fundamental components of the point of common coupling (PCC) voltage and the converter output current from two adjacent single-cycle windows. By combining the voltage equations of the two windows, the unknown equivalent grid voltage components are eliminated, and the grid resistance and reactance can be calculated without injecting additional perturbations or using external phasor measurement equipment. Under constant-current conditions, a simulation with a sudden change in grid impedance is used to verify the effectiveness of the method. Experiments are carried out on a three-phase three-wire energy storage converter under current-step and impedance-switching conditions. The results show that the estimated grid resistance and reactance have small differences from the preset values. The estimation errors of the resistance and reactance on the α-axis are 5.78% and 5.27%, respectively, while those on the β-axis are 0.27% and 1.60%, respectively. This shows that the proposed method can achieve accurate online grid impedance estimation without interfering with the normal operation of the converter, and can improve the stability and adaptive control capability of the energy storage converter.

Keywords: impedance estimation; non-intrusive estimation; energy storage converter; synchronization stability; power regulation; sliding-window discrete Fourier transform

1. Introduction

The energy storage converter can quickly control the power of the energy storage system and can conduct two-way power flow. The fast response nature of the energy storage converter at the millisecond level allows the energy storage systems to regulate power generation fluctuations, take part in frequency and voltage control, and improve the flexibility of power systems [1]. With an increase in renewable energy penetration and use of power electronics-based equipment, the relationship between converters and grid has become more important. Changes in grid impedance affect the stability, performance, and weak grid capabilities of converters [2,3].

When renewable energy generation and energy storage systems are connected through power electronic converters, power fluctuations and interactions among parallel converters can alter the dynamic characteristics of the grid-connected system [4, 5]. In weak grids, large grid impedance can interact with the phase-locked loop (PLL) and converter control dynamics, reducing the stability margin and increasing the risk of oscillation [6]. Harmonic interactions and converter-grid coupling can further aggravate these problems [7, 8]. Previous studies have investigated the influence of grid impedance from the aspects of impedance-based stability criteria, phase-locked-loop synchronization stability, virtual impedance [9–11], sequence-domain modeling, and harmonic stability [12–14]. Accurate grid impedance information is essential for the safe operation and stable control of grid-connected energy storage converters.

Nonintrusive and measurement-based techniques can also be used to determine Thevenin equivalent parameters by making use of passive phasor measurements. The first technique was suggested by Su and Liu [15], which is a phasor measurement unit (PMU)-based approach for estimation of Thevenin equivalent parameters. The second technique is based on graphical manipulation of phasors and was proposed by Abdelkader et al. [16].

Xie et al. [17] applied the recursive least squares (RLS) method to estimate the equivalent parameters of the external network. Vu et al. [18] used locally measured data to estimate the Thevenin equivalent parameters and assess the voltage stability margin. Ohtsuka et al. [19] used continuously sampled data to calculate the equivalent grid reactance and then performed dynamic estimation using a Kalman filter. However, neglecting grid resistance reduces the estimation accuracy in resistive or low-voltage networks. Li et al. [20] used voltage and current data from three adjacent sampling cycles to estimate the impedance. These methods require root-mean-square values, power, or additional phasor information for estimation. Such information may depend on measurement and calculation approaches such as PMUs, which are costly and complex.

Abdi et al. [21] modified the network impedance matrix and introduced a sensitivity-based correction method. This method obtains wide-area voltage and current phasors and network model information, and uses phasor measurements to estimate the Thevenin equivalent circuits observed from multiple buses. However, it has high requirements for measurement, communication, and modeling.

Impedance information is essential for converter control, grid strength assessment, and stability analysis, but existing methods still require training data or relatively complex estimation and modeling procedures. Short-circuit equivalent models for an external grid with inverter-interfaced sources have been studied by Xie and Xiao [22]. Pandurangan et al. [23] presented a real-time approach to compute grid impedance and analyzed the impact of grid impedance variation on converter performance. Kim et al. [24] computed the impedance of the line between the point of interconnection and the measuring point, for reactive power control applications. Mohammed et al. [25] suggested a data-driven approach to identify the impedance model of an inverter under different operating conditions. Hou et al. [26] studied equivalent modeling approaches for the evaluation of the strength of grid-connected and hybrid grid-connected systems.

Hoffmann and Fuchs [27] used extended Kalman filter to compute the equivalent impedance of the grid, but the use of harmonic differential equations increased the computational burden.

The dynamic characteristics of the converter controller may also introduce phase errors and affect the accuracy of grid impedance estimation [28]. The above methods show that the Thevenin equivalent parameters can be estimated from naturally occurring operating data without injecting specific estimation perturbations [15,16,21]. However, existing methods still face some challenges. Some methods neglect the resistance component and only estimate the inductive component of the grid impedance, while other methods require PMU data, power measurements, or complex state estimation models. During power command adjustment and operating mode switching, energy storage converters inevitably undergo current regulation transients. These transients can provide natural excitation for impedance estimation without additional test signals.

In order to solve these problems, the current research work has proposed a non-intrusive approach for estimating the grid impedance using the sliding-window discrete Fourier transform (DFT). In this case, the fundamental components of voltage and current at the point of common coupling (PCC) are estimated by the DFT using two adjacent single-cycle windows. The unknown grid voltage components are eliminated using the algebraic approach, thus allowing the calculation of grid resistance and reactance from the local measurements of PCC voltage and converter output current.

A notable feature of the proposed method is that it does not require artificially injected perturbations. Unlike recursive parameter estimation and state estimation methods, which usually require iterative updates of parameters or states, this method uses the fundamental voltage and current components from two adjacent sampling cycles and eliminates the unknown equivalent grid voltage components to derive explicit algebraic expressions for the grid resistance and reactance. In addition, the method includes two complementary calculation branches. When the converter output current changes while the grid impedance remains approximately unchanged, the method estimates the absolute grid resistance and reactance. When the converter output current remains approximately unchanged but the grid impedance changes, the incremental resistance and reactance can be calculated from the corresponding changes in the PCC voltage. Therefore, both normal converter power regulation transients and naturally occurring grid impedance changes can be incorporated into a unified estimation framework.

The proposed method has been compared to other methods with regard to the impedance components estimated, the excitation sources used, the criterion used for the validation of excitation, and the harmonic performance in **Table 1**. This shows the strengths of the proposed method in terms of using voltage normalization and current variation thresholds in order to avoid erroneous updates in case of poor excitation, and also in estimating fundamental voltage and current components using DFT.

Unlike the PMU-based method that is used for a wide area [21], this approach does not need a network impedance matrix or synchronized phasor measurement of the whole system. Moreover, unlike the data-driven method, this approach does not involve offline training of the model or any training data. The impedance of the grid can be estimated based on local PCC voltage and converter current during two consecutive fundamental cycle windows.

Table 1. Comparison of the proposed method with representative grid impedance estimation methods.

Method	Excitation-validity criterion	Estimated impedance	Excitation source	Performance under harmonics
RLS [17]	/	x & r	Natural variation	Limited
Kalman filter [19]	/	x only	Natural variation	Limited
Wide-area PMU-based TE estimation [21]	/	x & r	Normal operating data and wide-area PMUs	Not specifically addressed
Extended Kalman filter [27]	/	x & r	Natural variation	Requires harmonic modeling
Data-driven [25]	Depends on training-data coverage	x & r	Training data	Depends on the training dataset
Proposed method	Set thresholds	x & r	Inherent power regulation	Good

The main contributions of this paper are summarized as follows. Explicit algebraic expressions for the grid resistance and reactance are derived by eliminating the unknown equivalent grid voltage components from the voltage equations of two adjacent fundamental-cycle windows. A unified estimation procedure is established for current changes and impedance changes, providing absolute and incremental grid impedance information, respectively. The grid resistance and reactance are calculated using only the locally sampled PCC voltage and converter output current, without additional perturbation injection, external phasor measurement equipment, iterative state estimation, or offline model training.

2. Materials and methods

2.1. System description

The grid-connected energy storage system considered in this paper is shown in **Figure 1**.

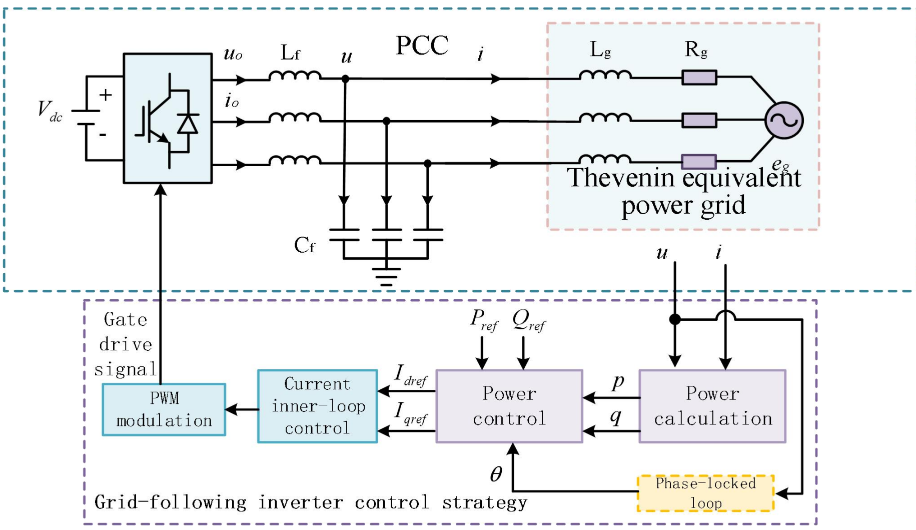

Figure 1. System diagram of the grid-connected energy storage converter.

The system mainly consists of a direct-current energy storage source, a power electronic converter, an output filter, a point of common coupling (PCC), and the equivalent power grid. The power grid is represented by a Thevenin equivalent voltage source connected in series with the grid resistance and inductive reactance. These impedance parameters may vary with the grid structure, operating condition, transmission line configuration, and connection status of nearby equipment.

The energy storage converter adopts a grid-following control strategy. The phase-locked loop obtains the grid-voltage phase angle from the measured PCC voltage and provides the synchronization reference for the control system. The active- and reactive-power commands are converted into current references through the outer power-control loop. The inner current-control loop then regulates the converter output current, and the pulse-width modulation module generates the gate-drive signals for the switching devices. In this way, the converter can control the magnitude and phase of the injected current and realize bidirectional power exchange between the energy storage unit and the power grid.

Although the PCC voltage and converter output current can be measured directly, the equivalent grid voltage behind the grid impedance cannot be obtained from local measurements. In addition, the resistance and reactance between the PCC and the equivalent grid source are generally unknown and may change during system operation. These parameters directly influence the voltage response at the PCC and the dynamic interaction between the converter and the grid. Therefore, their online estimation is important for stability assessment, adaptive parameter tuning, and weak-grid operation.

The proposed method uses only the sampled PCC voltage and converter output current. The fundamental components of these signals are extracted by the sliding-window discrete Fourier transform, and the equivalent grid resistance and reactance are then estimated from the relationship between two adjacent sampling periods. No additional disturbance-injection device or external phasor measurement unit is required.

2.2. Grid impedance estimation model

From the perspective of the point of common coupling, the external power grid can be represented by the Thevenin equivalent circuit shown in **Figure 2**. The equivalent model consists of an ideal grid-voltage source and a series grid impedance.

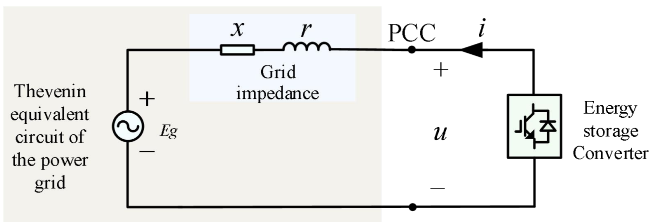

Figure 2. Thevenin equivalent circuit model of the grid.

In **Figure 2**, E_g denotes the equivalent grid electromotive force, r and x denote the equivalent grid resistance and reactance, respectively, u denotes the voltage at the PCC, and i denotes the current injected into the grid by the energy storage converter. The complex grid impedance is expressed as $Z_g = r + jx$, and its magnitude is denoted by $|Z_g|$.

Since the voltage behind the grid impedance cannot be measured directly, the values of *r* and *x* must be determined from the locally sampled PCC voltage and converter output current.

The data acquisition system samples the three-phase PCC voltage and converter output current. The sampled three-phase voltage and current signals are transformed into the stationary $\alpha\beta$ reference frame using the Clarke transformation, and the sliding-window DFT is applied over one fundamental cycle. Assuming that the sampling frequency is f_s, the grid fundamental frequency is f_1, and the sampling interval is $\Delta t = 1/f_s$, the number of sampling points within one fundamental cycle is $n = f_s/f_1$. The phase angle of the fundamental voltage component is calculated as follows:

$$\tan\varphi = \frac{U_\beta}{U_\alpha} \tag{1}$$

where U_α and U_β are the sine and cosine components, respectively, obtained by applying the sliding-window DFT to the sampled voltage $u(i\Delta t)$. These components are calculated as follows:

$$\begin{cases} U_\alpha = \frac{2}{n}\sum_{i=0}^{n-1} u(i\Delta t)\sin(2\pi i\Delta t/n) \\ U_\beta = \frac{2}{n}\sum_{i=0}^{n-1} u(i\Delta t)\cos(2\pi i\Delta t/n) \end{cases} \tag{2}$$

Similarly, the phase angle of the fundamental current component is calculated as follows:

$$\tan\gamma = \frac{I_\beta}{I_\alpha} \tag{3}$$

The phase-angle difference between the PCC voltage and the converter output current can be expressed as:

$$\tan(\varphi-\gamma) = \frac{\frac{U_\beta}{U_\alpha} - \frac{I_\beta}{I_\alpha}}{1 + \frac{U_\beta}{U_\alpha}\frac{I_\beta}{I_\alpha}} = \frac{U_\beta I_\alpha - I_\beta U_\alpha}{U_\beta I_\beta + U_\alpha I_\alpha} \tag{4}$$

The magnitudes of the fundamental voltage and current phasors are denoted by U and I, respectively. Accordingly, the magnitude of the equivalent grid impedance can be calculated as follows:

$$|Z_g| = \frac{U}{I} = \frac{\sqrt{U_\alpha^2 + U_\beta^2}}{\sqrt{I_\alpha^2 + I_\beta^2}} \tag{5}$$

U and I denote the magnitudes of the voltage and current phasors, respectively. The phasor decomposition of Z_g is shown in **Figure 3**.

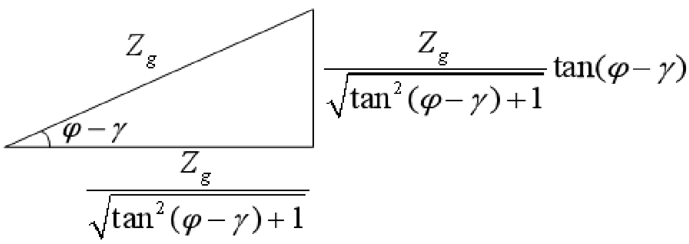

Figure 3. Geometric decomposition of the grid-impedance phasor.

According to **Figure 3**, the equivalent resistance and reactance are related to the impedance magnitude and the voltage-current phase-angle difference as follows.

$$x = |Z_g| \sin(\varphi - \gamma) = \frac{U_\beta I_\alpha - U_\alpha I_\beta}{I_\alpha^2 + I_\beta^2} \tag{6}$$

$$r = |Z_g| \cos(\varphi - \gamma) = \frac{U_\alpha I_\alpha + U_\beta I_\beta}{I_\alpha^2 + I_\beta^2} \tag{7}$$

The phasor relationships among the PCC voltage, converter output current, and equivalent grid voltage are illustrated in **Figure 4**.

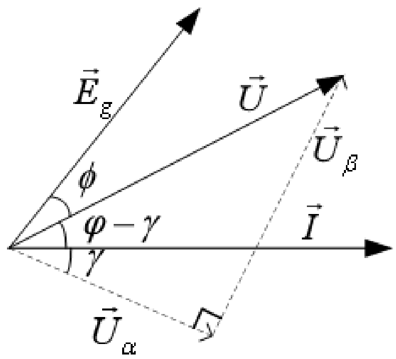

Figure 4. Phasor relationships among the PCC voltage, converter output current, and equivalent grid voltage.

According to Kirchhoff's voltage law, the PCC voltage, converter output current, equivalent grid voltage, and grid impedance satisfy the vector relationship:

$$E_g = U - IZ_g = U - I(r + jx) \tag{8}$$

By separating the real and imaginary parts of Equation (8), the grid impedance estimation model can be written as:

$$\begin{cases} E_{g\alpha} = U_\alpha + I_\beta x - I_\alpha r \\ E_{g\beta} = U_\beta - I_\alpha x - I_\beta r \end{cases} \tag{9}$$

Within a single sampling cycle, Equation (9) contains four scalar unknowns, namely, $E_{g\alpha}$, $E_{g\beta}$, r, and x, but only two scalar equations are available. Therefore, the equations are insufficient to determine all the unknowns. It can be assumed that the equivalent grid voltage phasor E_g, grid resistance r, and grid reactance x remain essentially unchanged over two adjacent cycles, while the PCC voltage and converter output current are allowed to vary, so that the equations can be solved.

2.3. Grid impedance estimation method

Based on the assumption introduced in Section 2.2, voltage and current data from two consecutive sampling periods are used to estimate the grid impedance. To distinguish the data obtained in the two periods, the superscript "–" denotes the voltage and current components of the previous period. Thus, $U_\alpha{}^-$, $U_\beta{}^-$, $I_\alpha{}^-$, and $I_\beta{}^-$ represent the corresponding components in the previous period, whereas U_α, U_β, I_α, and I_β denote those in the current period. The equivalent grid-voltage phasor E_g, grid resistance r, and grid reactance x are assumed to remain approximately unchanged over the two adjacent periods.

Because the equivalent grid voltage cannot be measured directly, its contribution must be eliminated before the grid impedance can be calculated using locally measured voltage and current data. By combining the real- and imaginary-axis equations corresponding to the two adjacent periods, the unknown equivalent grid-voltage component can be eliminated. To derive the grid-impedance calculation equations, Equation (9) is first written for the previous fundamental-period window, as given in Equation (10). The equations for the current and previous windows are then subtracted to eliminate the unknown equivalent grid-voltage components. The detailed elimination process is given below.

According to Equation (9), the previous fundamental-period window can be expressed as:

$$\begin{cases} E_{g\alpha} = U_\alpha^- + I_\beta^- x - I_\alpha^- r \\ E_{g\beta} = U_\beta^- - I_\alpha^- x - I_\beta^- r \end{cases} \tag{10}$$

Because $E_{g\alpha}$, $E_{g\beta}$, r, and x are assumed to remain approximately unchanged over the two adjacent periods, subtracting Equation (10) from Equation (9) eliminates the equivalent grid-voltage components and gives Equation (11).

$$\begin{cases} \left(I_\beta - I_\beta^-\right) x - \left(I_\alpha - I_\alpha^-\right) r = -\left(U_\alpha - U_\alpha^-\right) \\ -\left(I_\alpha - I_\alpha^-\right) x - \left(I_\beta - I_\beta^-\right) r = -\left(U_\beta - U_\beta^-\right) \end{cases} \tag{11}$$

By multiplying and combining these two equations, the following simultaneous equations are obtained:

$$\begin{cases} \dfrac{I_1 x + I_2 r = U_2}{-I_2 x + I_1 r = U_1} \end{cases} \tag{12}$$

where:

$$\begin{cases} I_1 = I_\alpha^2 + I_\beta^2 - I_\alpha I_\alpha^- - I_\beta I_\beta^- \\ I_2 = I_\beta I_\alpha^- - I_\alpha I_\beta^- \\ U_1 = \left(U_\alpha - U_\alpha^-\right) I_\alpha + \left(U_\beta - U_\beta^-\right) I_\beta \\ U_2 = \left(U_\beta - U_\beta^-\right) I_\alpha - \left(U_\alpha - U_\alpha^-\right) I_\beta \end{cases} \tag{13}$$

The resulting grid impedance estimation equations are expressed as:

$$\begin{cases} \left(I_\alpha^2 + I_\beta^2 - I_\alpha I_\alpha^- - I_\beta I_\beta^-\right) x \\ \quad + \left(I_\beta I_\alpha^- - I_\alpha I_\beta^-\right) r \\ = \left(U_\beta - U_\beta^-\right) I_\alpha - \left(U_\alpha - U_\alpha^-\right) I_\beta \\ \left(I_\alpha^2 + I_\beta^2 - I_\alpha I_\alpha^- - I_\beta I_\beta^-\right) r \\ \quad - \left(I_\beta I_\alpha^- - I_\alpha I_\beta^-\right) x \\ = \left(U_\alpha - U_\alpha^-\right) I_\alpha + \left(U_\beta - U_\beta^-\right) I_\beta \end{cases} \tag{14}$$

The grid impedance calculation formulas can be obtained as:

$$x = \frac{I_1 U_2 - I_2 U_1}{I_1^2 + I_2^2} \tag{15}$$

$$r = \frac{I_1 U_1 + I_2 U_2}{I_1^2 + I_2^2} \tag{16}$$

Equations (15) and (16) show that both the grid resistance and reactance can be obtained from the fundamental voltage and current components of two adjacent sampling periods. The required variations can be generated naturally by a change in the converter output-current reference, charge–discharge power regulation, or another normal operating transition. For this reason, there is no need for any further disturbance to be introduced in voltage or current in the power grid.

The validity of the estimation algorithm will depend on whether there are some differences in voltage and current values during the two sampling intervals. In case the values do not change much, the denominator in Equations (15) and (16) becomes very small, and hence leads to the estimation results becoming invalid. In practice, the estimation result is calculated when there is a noticeable change in voltage value or phase.

A second operating condition must also be considered. When the converter output current remains unchanged but the grid impedance changes, the absolute grid impedance cannot be recalculated from the current variation because no current excitation is available. However, the change in the PCC voltage reflects the change in the voltage drop across the grid impedance. Under this condition, the incremental grid reactance and resistance can be calculated as:

When the converter output current remains unchanged while the grid impedance varies, the current components satisfy the following relationship:

$$\begin{cases} I_\alpha = I_\alpha^- \\ I_\beta = I_\beta^- \end{cases} \tag{17}$$

The changes in impedance and voltage between the current and previous cycles are defined as:

$$\begin{cases} \Delta x = x - x^- \\ \Delta r = r - r^- \\ \Delta U_\alpha = U_\alpha - U_\alpha^- \\ \Delta U_\beta = U_\beta - U_\beta^- \end{cases} \tag{18}$$

Subtracting the α-axis equation for the previous cycle from that for the current cycle yields:

$$\Delta U_\alpha + I_\beta \Delta x - I_\alpha \Delta r = 0 \tag{19}$$

Similarly, subtracting the β-axis equations gives:

$$\Delta U_\beta - I_\alpha \Delta x - I_\beta \Delta r = 0 \tag{20}$$

Therefore,

$$\begin{cases} I_\beta \Delta x - I_\alpha \Delta r = -\Delta U_\alpha \\ -I_\alpha \Delta x - I_\beta \Delta r = -\Delta U_\beta \end{cases} \tag{21}$$

Solving these two simultaneous equations gives:

$$\Delta x = \frac{\left(U_\beta - U_\beta^-\right) I_\alpha - \left(U_\alpha - U_\alpha^-\right) I_\beta}{I_\alpha^2 + I_\beta^2} \tag{22}$$

$$\Delta r = \frac{\left(U_\alpha - U_\alpha^-\right) I_\alpha + \left(U_\beta - U_\beta^-\right) I_\beta}{I_\alpha^2 + I_\beta^2} \tag{23}$$

According to Equations (22) and (23), the incremental reactance and resistance can be calculated from the change in the PCC voltage.

Here, *Δx* and *Δr* denote the changes in grid reactance and resistance between the two adjacent periods, respectively. Positive values indicate an increase in the corresponding impedance component, whereas negative values indicate a decrease. This incremental calculation allows the method to detect a grid-impedance variation even when the converter output current is maintained at a constant value.

The complete implementation procedure is shown in **Figure 5**.

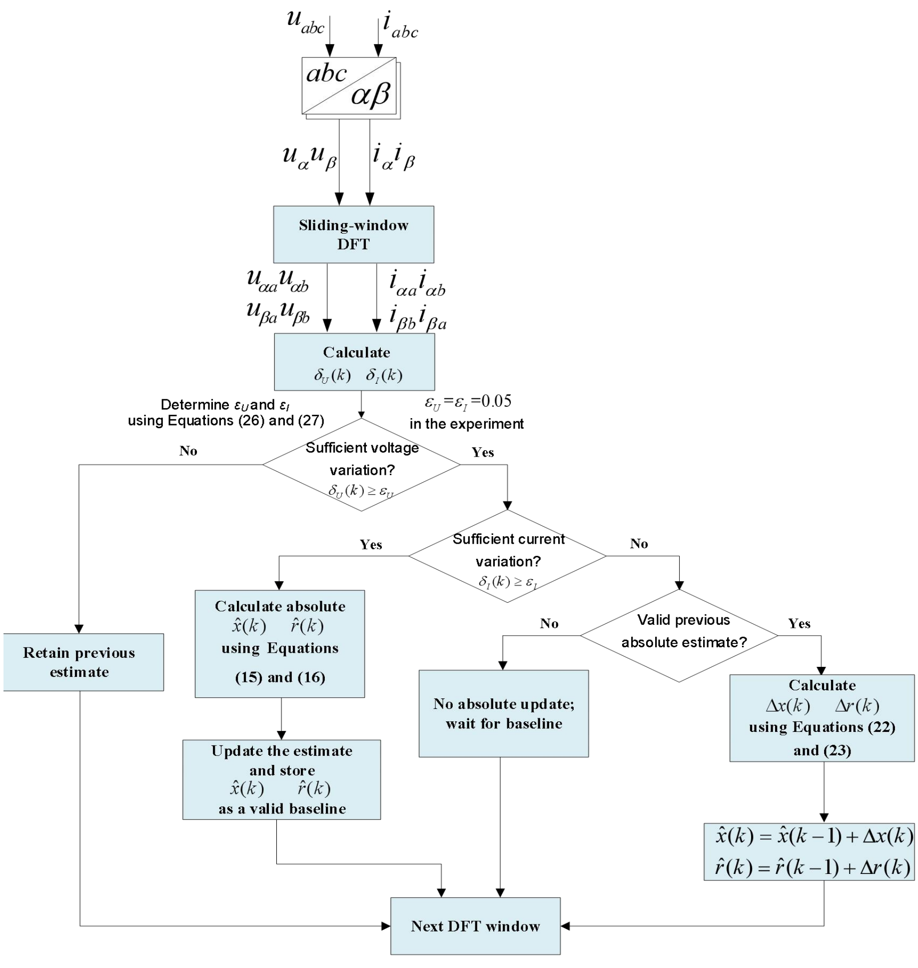

Figure 5. Flowchart of the proposed non-intrusive grid impedance estimation method based on sliding-window DFT.

The data acquisition system samples the three-phase PCC voltage and converter output current. These signals are transformed into the stationary $\alpha\beta$ reference frame using the Clarke transformation, and the fundamental sine and cosine components of the voltage and current are extracted using the sliding-window DFT algorithm.

The changes in the fundamental voltage and current vectors between two adjacent cycles are defined as:

$$\delta_U(k) = \frac{\left|\widehat{U}(k) - \widehat{U}(k-1)\right|}{U_N} \tag{24}$$

$$\delta_I(k) = \frac{\left|\widehat{I}(k) - \widehat{I}(k-1)\right|}{I_N} \tag{25}$$

where $\widehat{U}(k)$ and $\widehat{I}(k)$ denote the fundamental voltage and current phasors obtained from the current DFT window, respectively, and U_N and I_N are the voltage and current base values used for normalization. For the experimental implementation, U_N = 20 V and I_N = 5 A. The phasor differences account for changes in both magnitude and phase.

The voltage and current detection thresholds are denoted by ε_U and ε_I, respectively. They are determined from the steady-state fluctuations measured during initialization. Each threshold is defined as the mean of the corresponding normalized variation plus three times its standard deviation.

$$\varepsilon_U = \bar{\delta}_U + 3\sigma_{\delta U} \tag{26}$$

$$\varepsilon_I = \bar{\delta}_I + 3\sigma_{\delta I} \tag{27}$$

In the present laboratory experiment, the normalized voltage and current variation thresholds are both set to 0.05. A variation reaching 5% of the base value is regarded as sufficient excitation.

When $\delta_U < \varepsilon_U$ is satisfied, the voltage variation is small, and the previous impedance estimation result remains unchanged. When $\delta_U \geq \varepsilon_U$ is satisfied, the voltage response is sufficient, and the magnitude of the current variation is evaluated.

If $\delta_I \geq \varepsilon_I$ is satisfied, the current variation meets the requirement. The absolute grid impedance is then calculated using Equations (15) and (16), respectively, and taken as the estimation result. The corresponding data are also stored as the new valid reference data for subsequent incremental calculations.

If $\delta_I < \varepsilon_I$ is satisfied, the converter output current remains essentially unchanged, but the detected PCC voltage variation indicates a possible change in the grid impedance. The algorithm first checks whether a valid impedance estimation result is available. If so, the incremental grid reactance and resistance are calculated using Equations (22) and (23), respectively, and the impedance estimation result is updated.

$$\widehat{x}(k) = \widehat{x}(k-1) + \Delta x(k) \tag{28}$$

$$\widehat{r}(k) = \widehat{r}(k-1) + \Delta r(k) \tag{29}$$

$\widehat{x}(k-1)$ and $\widehat{r}(k-1)$ denote the latest valid impedance estimates, respectively. If no valid absolute baseline is available, the absolute impedance estimate is not updated, and the algorithm waits for a valid initial value. Only after all branches have been completed does the algorithm proceed to the next DFT window and continue operating.

3. Results and discussion

3.1. Simulation verification

A simplified single-phase full-bridge inverter model was established to preliminarily verify the proposed incremental grid impedance estimation method. The purpose of the simulation was to determine whether a change in grid impedance could be estimated when the converter output current remained approximately constant. This condition corresponds to the incremental impedance calculation described by Equations (22) and (23).

The DC-side bus voltage of the inverter was set to 50 V, and the amplitude of the alternating-current (AC) grid voltage was set to 25 V. The inverter was connected to the equivalent grid through a line containing resistance and inductance. A controllable switch was used to change the line impedance during operation. Before 0.1 s, an additional resistance of 2 Ω and an inductance of 2 mH were connected in series with the grid. At 0.1 s, the switch was closed, bypassing these components. Therefore, the grid-side resistance and inductance decreased by 2 Ω and 2 mH, respectively.

During the switching process, the converter current reference remained unchanged. The current controller maintained the output current close to its original value, while the change in grid impedance mainly caused a variation in the PCC voltage. Since the current components in two adjacent periods remained approximately unchanged, the incremental resistance and reactance were calculated from the voltage variation using Equations (22) and (23).

For each DFT update performed through a valid sliding window technique, the impedance values are computed and recorded. Thus, the impedance curves as shown in **Figure 6** represent both the pre- and post-switching data as well as the dynamic online calculation process of the grid impedance. **Figure 6** shows the voltage and current waveforms along with the calculated and theoretical values of incremental resistance and reactance. The dotted vertical line at 0.1 s represents the time at which switching occurs to the grid impedance.

Before the switching instant, the grid impedance remained unchanged, and the calculated incremental resistance and reactance were close to zero. At 0.1 s, the switch was closed, producing a detectable change in the PCC voltage, while the output current remained approximately constant. The sliding-window DFT extracted the fundamental voltage and current components, and the algorithm entered the incremental impedance calculation branch.

The switching of grid impedance at 0.1 s will result in the transient inclusion of sample points for both pre- and post-switching operating conditions within the one-cycle sliding window DFT. Assuming that the grid frequency is 50 Hz, the size of the DFT window is 20 ms. Therefore, the incrementally computed resistance and reactance values start to reflect the post-switching operating condition after about one fundamental period and stabilize after about 0.12 s. The resulting delay is due to the finite size of the DFT window and not due to iteration.

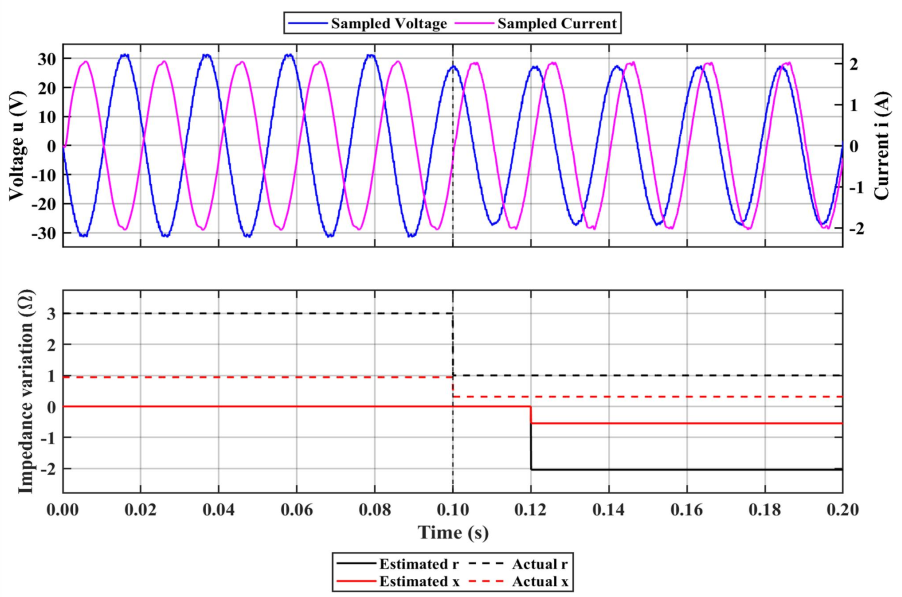

Figure 6. Simulation results of incremental grid impedance estimation under constant output current and grid-impedance switching.

The theoretical change in resistance is −2 Ω, while the theoretical change in reactance corresponding to a 2 mH inductance variation at 50 Hz is approximately −0.628 Ω. The final calculated incremental resistance is −2.0565 Ω, and the calculated incremental reactance is approximately −0.54 Ω. The negative sign in both cases indicates the decrease in the impedance component values. The rest of the error is mainly due to the effect of sampling, limited DFT window, switching transients, and truncation.

3.2. Experimental verification

To further verify the proposed method, an experimental platform based on a three-phase three-wire energy storage converter was established, as shown in **Figure 7**. The platform mainly consists of a DC power supply, a three-phase converter, an output filter, voltage and current sampling circuits, a control unit, an autotransformer, and the grid-side impedance network. The energy storage converter transfers power to the AC source through the autotransformer. A controllable switch is connected in parallel with an additional grid-side resistance and inductance so that the equivalent line impedance can be changed during the experiment.

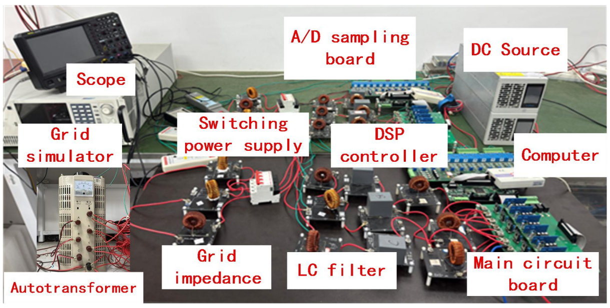

Figure 7. Experimental platform of the grid-connected DC/AC energy storage converter.

The three-phase PCC voltages and converter output currents are sampled by the control system. The measured three-phase quantities are transformed into the stationary $\alpha\beta$ reference frame using the Clarke transformation. The α- and β-axis voltage and current components are then processed separately by the sliding-window DFT. Because the experimental grid is approximately symmetrical, the grid impedance estimated from the α- and β-axis components should theoretically be consistent. The comparison between the two axes can therefore also be used to evaluate the repeatability of the estimation method.

The actual equivalent impedance of the autotransformer and the original connection line cannot be measured accurately as a single known parameter. Therefore, a differential verification method is adopted. When the switch is closed, the additional resistance and inductance are bypassed. When the switch is opened, a resistance of 2 Ω and an inductance of 2 mH are inserted into the grid-side line. The proposed algorithm is executed under both switching states, and the difference between the two estimation results is compared with the known additional impedance. In this way, the influence of the unknown initial grid and transformer impedance can be eliminated from the verification process.

The main experimental parameters are listed in **Table 2**.

Table 2. Experimental parameters of the energy storage converter.

Parameter item	Parameter value
Additional grid resistance	2.0 Ω
Additional grid inductance	2.0 mH
Rated output current	5 A
DC bus voltage	50 V
Converter output filter inductor L	2.0 mH
Switching frequency	12.8 kHz
Grid voltage amplitude	20 V
Grid fundamental frequency	50 Hz
Sampling frequency	12.8 kHz
Sliding-window DFT length	256 samples (20 ms)

The rated converter output current is 5 A, the DC bus voltage is 50 V, and the converter-side filter inductance is 2 mH. The switching frequency and sampling frequency are both selected according to the control and data-processing requirements of the prototype. The grid-voltage amplitude is 20 V. The inserted grid resistance and inductance are 2 Ω and 2 mH, respectively. At a fundamental frequency of 50 Hz, the 2 mH inductance corresponds to an inductive reactance of approximately 0.628 Ω.

The converter control and impedance estimation algorithm are implemented on a DSP-based control platform using a TMS320F28335 processor. The PCC voltage and converter output current are measured using CHV-25P Hall-effect voltage sensors and CHB-25NP Hall-effect current sensors, respectively. The system employs two ADS8556IPM analog-to-digital converters. One acquires the three-phase voltage signals, while the other acquires the three-phase current signals. Both converters are triggered by the same conversion start signal (CONVST), and identical filter parameters are used in the voltage and current signal-conditioning circuits. Therefore, the voltage and current channels are sampled synchronously at 12.8 kHz, minimizing differences in sampling time and phase delay between the measured voltage and current signals.

Grid synchronization was achieved using a PLL, with controller parameters K_{p_PLL} = 0.1 and K_{i_PLL} = 1. The converter output current was regulated by a PI controller in the *dq* synchronous reference frame, with controller parameters K_{p_PI} = 15 and K_{i_PI} = 85.

Sampling frequency was 12.8 kHz, while the grid fundamental frequency was 50 Hz. As a result, one cycle of the DFT included 256 sampling points and represented a time period of 20 ms. For each impedance estimation, two neighboring DFT windows were used.

The main computational burden of the proposed method arises from the extraction of the fundamental voltage and current components using the one-cycle DFT. For a direct implementation with n sampling points, the computational complexity of each DFT calculation is $O(n)$. After the fundamental components have been obtained, the impedance calculation using Equations (15), (16), (22), and (23) requires only a fixed number of scalar additions, multiplications, and divisions, corresponding to $O(1)$ complexity. Under the above sampling and window settings, the impedance estimation is performed at an interval of 40 ms. On the TMS320F28335 DSP, the DFT calculation for 256 sampling points requires approximately 0.8 ms, and the measured DSP computational-resource utilization is less than 2%. No matrix inversion, iterative optimization, covariance update, or offline model training is required. Only one cycle of voltage and current samples and the fundamental components obtained from the previous window need to be retained.

The first experiment verifies the absolute impedance estimation under a converter current-step condition. In the experiments, the impedance-estimation algorithm was also executed repeatedly over the complete recorded interval. The resistance and reactance values obtained at each valid DFT-window update were retained and plotted as continuous time-domain curves in **Figures 8** and **9**.

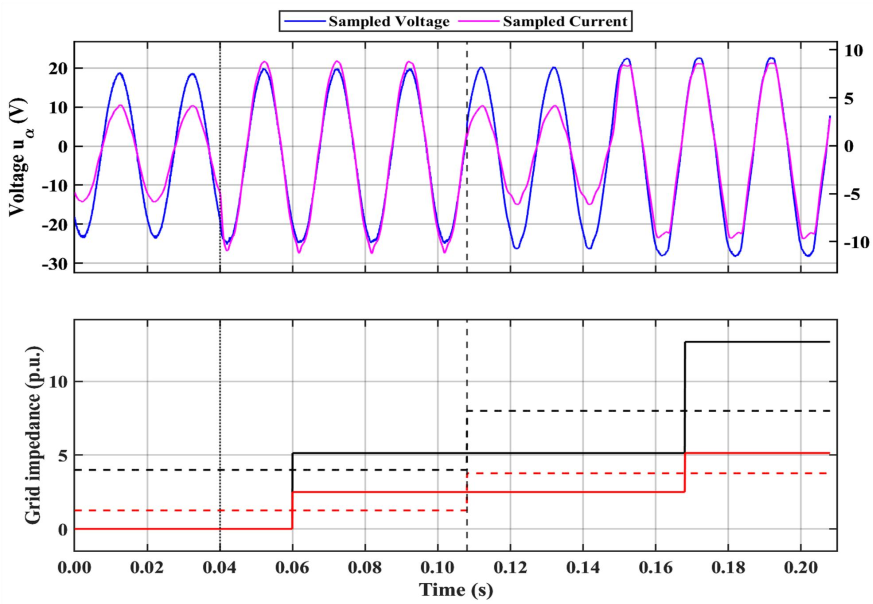

Figure 8. Experimental grid impedance estimation results under converter-current step and grid-impedance switching.

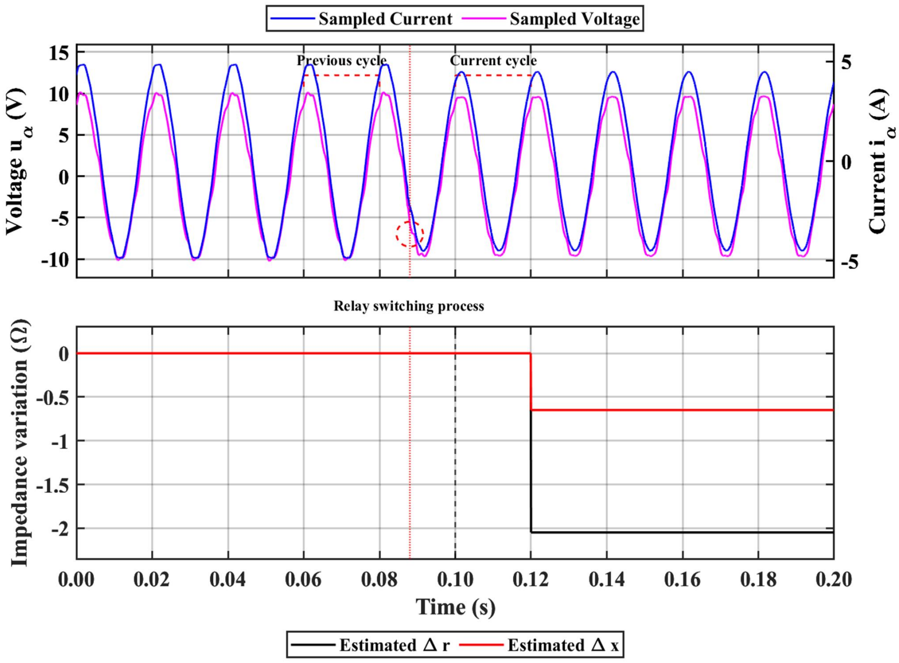

Figure 9. Experimental incremental impedance estimation results under constant output current and grid-impedance switching.

Figure 8 shows the α-axis voltage, current, estimated resistance, and estimated reactance. During the third fundamental cycle, the normal current regulation of the converter increases the current reference from 1 A to 2 A, rather than being triggered by an additional impedance estimation signal. This current step provides the natural excitation required by Equations (15) and (16).

The resistance and reactance curves in **Figure 8** are presented in per-unit values.

The voltage drop through the grid side resistor and inductor changes depending on the increase in the converter output current. Therefore, there will be slight change in the PCC voltage magnitude. The sliding-window DFT extracts the voltage and current components from two adjacent periods, and the grid resistance and reactance are calculated from their amplitude and phase relationships.

Because the impedance calculation uses the fundamental voltage and current components obtained from two adjacent one-cycle DFT windows, the resistance and reactance are not updated instantaneously after the current-reference change. At 50 Hz, the nominal data-window delay is approximately one fundamental period, corresponding to 20 ms. After the sliding window has completely entered the new operating condition, the calculated resistance and reactance stabilize. The practical settling process may be slightly longer because of the transient response of the converter current-control loop.

The parameters of the original transmission line, the autotransformer, the connecting wires, and any other parasitics before installing the supplementary impedance are estimated for the grid side. Therefore, the initial estimated impedance is slightly higher than the actual impedance of the line because of the above components. The difference does not affect the differential comparison since the original grid impedance is there even after the switching process.

It is at around 0.108 s that the switch shown in **Figure 7** gets switched open, resulting in an additional resistor of 2 Ω and an inductor of 2 mH being added to the circuit path on the grid side. After dampening the switching transient, the estimated total resistance increases to around 3.1697 Ω and the total reactance to around 1.2859 Ω. The incremental resistance and reactance introduced by the added components are determined by subtracting the pre-switching estimates from the post-switching values.

The differential estimation results are summarized in **Table 3**.

Table 3. Grid impedance estimation results and errors.

Parameter item	Actual value	Estimated value	Error
α-axis r	2.0 Ω	1.8844 Ω	5.78%
α-axis x	0.628 Ω	0.6611 Ω	5.27%
β-axis r	2.0 Ω	1.9946 Ω	0.27%
β-axis x	0.628 Ω	0.638 Ω	1.60%

For the α-axis, the estimated resistance difference is 1.8844 Ω, corresponding to an error of 5.78%, while the estimated reactance difference is 0.6611 Ω, corresponding to an error of 5.27%. For the β-axis, the estimated resistance difference is 1.9946 Ω, with an error of 0.27%, and the estimated reactance difference is 0.638 Ω, with an error of 1.60%. All four errors are below 6%, and the β-axis results are particularly close to the preset values.

The small difference between the α- and β-axis results may be caused by sampling-channel deviations, sensor gain errors, converter dead time, unbalanced parasitic parameters, and switching harmonics. In addition, the autotransformer and connecting conductors may introduce small asymmetries that are not included in the ideal three-phase impedance model. Nevertheless, the results from both axes correctly estimate the inserted resistance and reactance and demonstrate the effectiveness of the proposed absolute impedance estimation method.

A second experiment was conducted to verify the incremental impedance calculation when the converter output current remained approximately constant. There was no change in the reference signal throughout the duration of the experiment. The control system sent a command at $t = 0.08$ s for closing the circuit and bypassing the extra resistor and inductor. Due to the time lag in the switching system, the action took place about 10 ms after sending the command.

The corresponding experimental results are shown in **Figure 9**.

From the graph given in **Figure 9**, a lower grid impedance causes a change in the PCC voltage, although the output current of the converter remains almost unchanged. In this case, the formula for estimating the absolute impedances based on changes in current values cannot be applied since the current values in successive cycles remain almost constant. Thus, the incremental formula is used.

After the relay switching operation, the sliding-window DFT temporarily contains samples from both the pre-switching and post-switching operating conditions. Once the one-cycle window has fully entered the post-switching condition, the calculated incremental resistance and reactance become stable. At 50 Hz, the nominal update delay introduced by the DFT window is approximately 20 ms. The specific response observed in the figure also depends on the relay operating delay and the position of the switching instant relative to the sliding window.

The incremental resistance obtained is −2.0492 Ω while the incremental reactance is −0.6499 Ω. The negative values represent a decrease in resistance and reactance after bypassing the extra circuit components. This corresponds to the expected change of −2 Ω and −0.628 Ω, respectively.

The current-step experiment shows that the absolute grid resistance and reactance can be estimated from the inherent current regulation process of the converter. The impedance-switching experiment further demonstrates that impedance variations can still be estimated when the converter output current remains approximately constant. These results indicate that the natural operating variations of the energy storage converter can provide effective excitation for grid impedance estimation, allowing the required grid impedance information to be obtained without introducing additional estimation perturbations.

3.3. Robustness and applicability discussion

The derivation above assumes that E_g, r, and x remain approximately unchanged over the two consecutive fundamental-cycle windows used for one estimation. At 50 Hz, the two windows correspond to an observation interval of approximately 40 ms. This is a local stationarity assumption rather than an assumption that the grid remains unchanged throughout the entire operating process. It is applicable when the equivalent grid parameters vary slowly relative to this observation interval. If the grid parameters vary significantly within these two windows, this stationarity assumption is no longer satisfied.

The proposed method extracts the fundamental voltage and current components using a one-cycle sliding-window DFT. Under the nominal grid frequency and synchronous-sampling conditions, integer-order harmonic components are ideally orthogonal to the fundamental-frequency basis functions and therefore have a limited influence on the extracted fundamental components. The averaging operation within the DFT window also reduces the influence of random high-frequency measurement noise and switching ripple. However, these disturbances cannot be completely eliminated. When the natural voltage or current variation used for estimation is close to the background fluctuation level, the remaining noise may be amplified by the small denominator terms in Equations (15) and (16). The variation thresholds introduced in Section 2.3 are therefore required to prevent the impedance estimate from being updated under insufficient excitation.

The fixed threshold of 0.05 is used for the present experimental conditions. A threshold that is too low may increase the influence of measurement fluctuations, whereas a threshold that is too high may reduce the detection of valid excitation. For practical applications, the threshold can be adjusted adaptively according to the mean and standard deviation of the recent normalized voltage and current variations over a moving observation window.

Grid-frequency deviation is another important source of error. The present sliding-window DFT uses a window corresponding to one period at the nominal fundamental frequency. When the actual grid frequency deviates from the frequency used in the DFT calculation, the sampling window no longer contains an exact fundamental period. Spectral leakage may then cause amplitude and phase errors in the extracted voltage and current components, which are subsequently transferred to the calculated resistance and reactance. To quantitatively evaluate this effect, the grid frequency was varied while the other conditions remained unchanged, and the DFT calculation was still performed using the nominal frequency of 50 Hz. The corresponding estimation errors are listed in **Table 4**.

Table 4. Grid impedance estimation errors under different grid frequencies.

Grid frequency (Hz)	Frequency deviation	Resistance estimation error	Reactance estimation error
49.99	−0.02%	+0.50%	−10.67%
50.00	0	-0.50%	5.24%
50.01	+0.02%	-0.59%	19.89%

The resistance estimation error remains below 1% within the tested frequency range, while the reactance estimation error is more sensitive to the frequency deviation. For grids with noticeable frequency variation, the angular frequency and window length should be updated using the frequency estimated by the PLL or another frequency-tracking method.

The present derivation and experimental validation are based on an approximately balanced three-phase system. Under unbalanced grid-voltage conditions, positive- and negative-sequence components coexist in the stationary $\alpha\beta$ reference frame. Directly applying the proposed calculation to the mixed components may introduce periodic oscillations or bias into the impedance estimate. In such cases, positive-sequence extraction or sequence-component decomposition should be performed before the sliding-window DFT and impedance calculation.

To further verify the estimation method under unbalanced grid-voltage conditions, a numerical simulation was carried out. The peak values of the phase-A, phase-B, and phase-C grid voltages were set to 25 V, 20 V, and 30 V, respectively. Positive-sequence extraction was applied to the three-phase voltage and current signals before the sliding-window DFT and impedance calculation. The extracted positive-sequence voltage and current and the corresponding impedance estimation results are shown in **Figure 10**.

At 0.2 s, the grid resistance and reactance change by −2 Ω and −0.628 Ω, respectively. After the transient process, the estimated resistance and reactance variations converge to −1.9874 Ω and −0.5970 Ω, corresponding to estimation errors of 0.63% and 4.94%, respectively.

Measurement-channel errors also affect the estimation accuracy. Voltage- and current-sensor gain errors directly change the calculated impedance magnitude, while phase delay and asynchronous sampling between the voltage and current channels affect the calculated resistance and reactance. DC offsets may additionally cause leakage into the fundamental component. These effects can be reduced through sensor calibration, offset removal, synchronous sampling, and compensation for known channel delays. Converter dead time and switching nonlinearities introduce low-order harmonics and waveform distortion. Although the sliding-window DFT attenuates high-frequency switching components, low-order distortion near the fundamental frequency may still affect the estimation result.

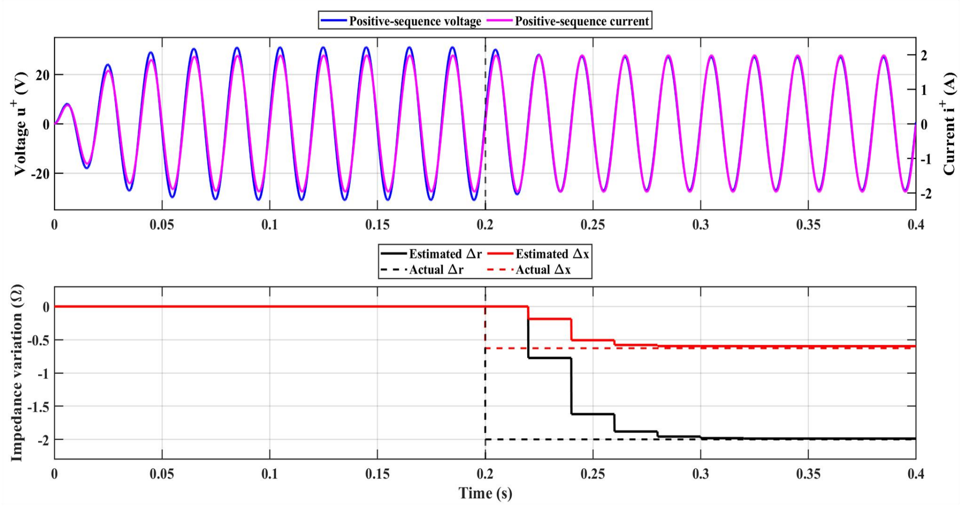

Figure 10. Simulation results of positive-sequence-based grid impedance estimation under unbalanced grid-voltage conditions.

When the proposed method is transferred from the present low-voltage laboratory platform to medium- and high-voltage systems, higher requirements are placed on voltage and current sensor accuracy and isolation, electromagnetic interference suppression, and channel synchronization. These practical factors should be considered in the implementation of the proposed method in higher-voltage systems.

4. Conclusion

This paper proposes a non-intrusive online grid impedance estimation method for energy storage converters based on the fundamental voltage and current components extracted using a sliding-window DFT. Normalized voltage and current variation criteria are introduced to evaluate whether the available excitation is sufficient. When the voltage and current variations are inadequate, the system retains the existing impedance estimates rather than performing an unreliable calculation.

The sliding-window DFT is also used to extract the fundamental voltage and current components effectively and reduce the influence of non-fundamental harmonic components under nominal-frequency and synchronous-sampling conditions. Both simulation and experimental results validate the effectiveness of the two calculation paths, and the estimated changes in resistance and reactance closely agree with the preset values.

The accuracy and dynamic response of the proposed method depend on the grid-frequency information used by the sliding-window DFT. The one-cycle data window introduces an inherent update delay. In practical applications, the DFT angular frequency and effective window length should therefore be updated using a sufficiently accurate and fast-responding PLL or another frequency-tracking method.

Author contributions: Conceptualization, YX; methodology, KL and CW; software, ZH; validation, CW; formal analysis, ZH; investigation, CW; data curation, HZ;

visualization, HZ; writing—original draft preparation, YX and ZH; writing—review and editing, KL; project administration, YX. All authors have read and agreed to the published version of the manuscript.

Funding: This research was funded by the Science and Technology Project of State Grid Integrated Energy Service Group Co., Ltd., "Research and Application of Optimized Operation and Coordinated Control Technology for Distribution Transformer Districts Integrating the Spatiotemporal Characteristics of Energy Storage", grant number 52789925000U.

Institutional review board statement: Not applicable.

Informed consent statement: Not applicable.

Data availability statement: The data supporting the findings of this study are available from the corresponding author upon reasonable request.

Conflict of interest: The authors declare no conflict of interest.

AI use statement: During the preparation of this work, the authors used ChatGPT (OpenAI) to improve the language, readability, and presentation of the manuscript. After using this tool, the authors carefully reviewed and edited the content as needed and take full responsibility for the content of the manuscript.

References

1. Wang G, Konstantinou G, Townsend CD, et al. A review of power electronics for grid connection of utility-scale battery energy storage systems. IEEE Transactions on Sustainable Energy. 2016; 7(4): 1778–1790. doi: 10.1109/TSTE.2016.2586941
2. Wen B, Dong D, Boroyevich D, et al. Impedance-based analysis of grid-synchronization stability for three-phase paralleled converters. IEEE Transactions on Power Electronics. 2016; 31(1): 26–38. doi: 10.1109/TPEL.2015.2419712
3. Cespedes M, Sun J. Adaptive control of grid-connected inverters based on online grid impedance measurements. IEEE Transactions on Sustainable Energy. 2014; 5(2): 516–523. doi: 10.1109/TSTE.2013.2295201
4. Chang F, Li Y, Peng Y, et al. A dual-layer cooperative control strategy of battery energy storage units for smoothing wind power fluctuations. Journal of Energy Storage. 2023; 70: 107789. doi: 10.1016/j.est.2023.107789
5. Rahman MM, Mohamed YARI. Dynamic interactions and stabilization of weak grid-tied parallel VSCs and parallel CSCs systems considering PVG dynamic resistance. IEEE Open Journal of Power Electronics. 2024; 5: 21–36. doi: 10.1109/OJPEL.2023.3340268
6. Kim KH, Cui S, Jung JJ. Current-oriented phase-locked loop method for robust control of grid-connected converter in extremely weak grid. IEEE Transactions on Power Electronics. 2024; 39(10): 11963–11968. doi: 10.1109/TPEL.2024.3419445
7. Liu J, Sun X, Chen Z, et al. A hybrid multiresonances suppression method for nonsynchronous LCL-type grid-connected inverter clusters under weak grid. IEEE Transactions on Power Electronics. 2024; 39(5): 5386–5399. doi: 10.1109/TPEL.2024.3366191
8. Zhang GR, Gao K, Xie RS, et al. Modeling and analysis of grid-connected inverter considering AC/DC harmonic coupling. Electrical Measurement & Instrumentation. 2024; 61(6): 72–79. (in Chinese)
9. Belkhayat M. Stability Criteria for AC Power Systems with Regulated Loads [PhD Thesis]. Purdue University; 1997.
10. Huang L, Xin H, Li Z, et al. Grid-synchronization stability analysis and loop shaping for PLL-based power converters with different reactive power control. IEEE Transactions on Smart Grid. 2020; 11(1): 501–516. doi: 10.1109/TSG.2019.2924295
11. Abdoli O, Gholipour M, Hooshmand RA. Improving synchronization stability of grid connected converters by virtual

impedance. IET Generation, Transmission & Distribution. 2021; 15(7): 1136–1143. doi: 10.1049/gtd2.12091

12. Rygg A, Molinas M, Zhang C, et al. A modified sequence-domain impedance definition and its equivalence to the dq-domain impedance definition for the stability analysis of AC power electronic systems. IEEE Journal of Emerging and Selected Topics in Power Electronics. 2016; 4(4): 1383–1396. doi: 10.1109/JESTPE.2016.2588733
13. Wang X, Blaabjerg F. Harmonic stability in power electronic based power systems: concept, modeling, and analysis. IEEE Transactions on Smart Grid. 2019; 10(3): 2858–2870. doi: 10.1109/TSG.2018.2812712
14. Kervyn de Meerendre M, Prieto-Araujo E, Ahmed KH, et al. Review of local network impedance estimation techniques. IEEE Access. 2020; 8: 213647–213661. doi: 10.1109/ACCESS.2020.3040099
15. Su HY, Liu TY. Robust Thevenin equivalent parameter estimation for voltage stability assessment. IEEE Transactions on Power Systems. 2018; 33(4): 4637–4639. doi: 10.1109/TPWRS.2018.2821926
16. Abdelkader SM, Eladl AA, Saeed MA, et al. Online Thévenin equivalent determination using graphical phasor manipulation. International Journal of Electrical Power & Energy Systems. 2018; 97: 233–239. doi: 10.1016/j.ijepes.2017.11.013
17. Xie SW, Hu ZJ, Wu FJ, et al. Static equivalent parameter identification method of multi-port external network based on recursive least squares algorithm. Power System Protection and Control. 2018; 46(3): 26–34. (in Chinese)
18. Vu K, Begovic MM, Novosel D, et al. Use of local measurements to estimate voltage-stability margin. IEEE Transactions on Power Systems. 1999; 14(3): 1029–1035. doi: 10.1109/59.780916
19. Ohtsuka K, Yokokawa S, Tanaka H, et al. An equivalent of multi-machine power systems and its identification for on-line application to decentralized stabilizers. IEEE Transactions on Power Systems. 1989; 4(2): 687–693. doi: 10.1109/59.193844
20. Li CY, Li SL, Wang WS, et al. Impact analysis of wind power grid and source fluctuations on equivalent impedance estimation and grid impedance online identification. Power System Technology. 2024; 48(6): 2376–2384. (in Chinese)
21. Abdi P, Hamedani-Golshan ME, Alhelou HH, et al. A PMU-based method for on-line Thévenin equivalent estimation. IEEE Transactions on Power Systems. 2022; 37(4): 2796–2807. doi: 10.1109/TPWRS.2021.3125007
22. Xie DX, Xiao SW. Short-circuit calculation equivalent of external power grid including inverter interfaced distributed generator and analysis of influencing factors. Power System Technology. 2024; 48(7): 2967–2976. (in Chinese)
23. Pandurangan R, Kaliannan P, Shanmugam P. Dynamic online grid impedance estimation and its effects on DC capacitor lifetime in variable frequency drive. IEEE Access. 2022; 10: 85243–85254. doi: 10.1109/ACCESS.2022.3197894
24. Kim WH, Kim YC, Song SH. Estimation and application for line impedance between IBR and POM. Energies. 2025; 18(12): 3135. doi: 10.3390/en18123135
25. Mohammed N, Zhou W, Ramasubramanian D, et al. Data-driven estimation of impedance of inverter-based resources for efficient stability evaluation. Electric Power Systems Research. 2025; 244: 111559. doi: 10.1016/j.epsr.2025.111559
26. Hou ZX, Li Y, Wang J, et al. Equivalent modeling method for grid-forming devices for strength assessment of grid-following/grid-forming hybrid systems. Automation of Electric Power Systems. 2025; 49(22): 90–100. (in Chinese)
27. Hoffmann N, Fuchs FW. Minimal invasive equivalent grid impedance estimation in inductive-resistive power networks using extended Kalman filter. IEEE Transactions on Power Electronics. 2014; 29(2): 631–641. doi: 10.1109/TPEL.2013.2259507
28. Yu JR, Liu WJ, Sun JW, et al. An improved grid impedance estimator for grid-forming converters in consideration of controller dynamics. International Journal of Electrical Power & Energy Systems. 2023; 154: 109424. doi: 10.1016/j.ijepes.2023.109424